ACS OMEGA

Open Access

http://pubs.acs.org/journal/acsodf

Article

Design of the Inhibitors for Pseudorabies Virus Replication by Reinforcement Learning from HSV-1 DNA Polymerase Inhibitors

Lin Wei,[#] Yang Hu,[#] Licheng Bai,[#] Chenxu Xiao, Zhang Liu, Yun You, Keke Wang, Yunyuan Huang, Junfei Zhu, Jun Weng, Wenling Zhou, Han Li, Honghe Zhao, Zhiyong Wu, Meng Mei, and Zigong Wei*

Cite This: *ACS Omega* 2025, 10, 3389−3397

Read Online

ACCESS | Metrics & More | Article Recommendations | Supporting Information

ABSTRACT: The reintroduction of the pseudorabies virus (PRV) has led to the emergence of epidemics in some pig farms in China, resulting in significant economic losses. Moreover, the number of human infections with PRV has increased. Therefore, research into the prevention and treatment of PRV strains is imperative. In this work, the PRV DNA polymerase (DNA pol) was found to exhibit a high degree of sequence and structural similarity to the herpes simplex virus 1 (HSV-1) DNA pol. Consequently, we provided the first experimental evidence that PNU-183792, a non-nucleoside inhibitor of HSV-1, inhibited PRV replication in cell assay, with an EC_{50} of 100 pM, providing the basis for further studies on PRV inhibitors. Then, with the great help of reinforcement learning, some new potential hits were discovered based on the HSV-1 DNA pol inhibitors. One of the compounds, **c14**, which showed significant anti-PRV potency and safety, with an EC_{50} of 14 pM and a CC_{50} of 343.7 μM, can be considered as a highly promising lead compound to support drug discovery and development for anti-PRV.

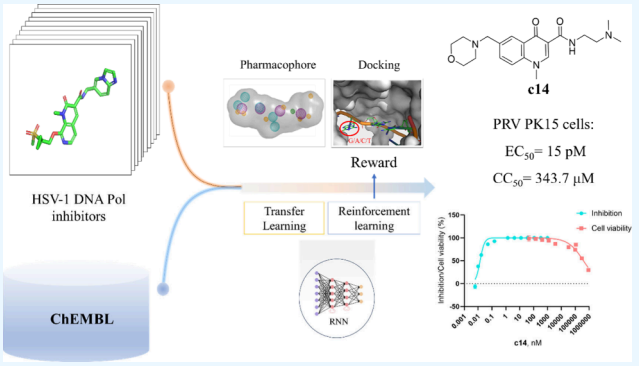

INTRODUCTION

The pseudorabies virus (PRV), also known as suid alphaherpesvirus 1 and Aujeszky's disease virus, is a DNA virus that primarily infects pigs, serving as its natural host. The name "pseudorabies" is derived from the resemblance of its symptoms to rabies.[1] It causes acute and virulent infectious diseases characterized by fever and encephalomyelitis, and piglets infected with PRV have an exceptionally high mortality rate of up to 100%.

A setback occurred at the end of 2011 when a new outbreak of PRV occurred in pig farms that had previously been immunized with the gene deletion vaccine (such as the Bartha-K61 strain).[2] There were reports of an increase in PRV positivity from 13.24% in 2012 to 31.03% in 2017 in 925 swine serum samples from 11 provinces in China.[3] In 2021, the results of molecular epidemiological investigations and analyses by researchers indicated that the predominant pseudorabies viruses in China were still traced back to the 2011 genotype II mutant strain. This continued prevalence illustrates the dynamic nature of PRV and emphasizes the necessity for consistent research and adaptation of control measures to effectively manage and mitigate the impact of PRV on the pig industry in China.

In addition to infecting pigs, PRV has the ability to infect a wide range of domestic and wild animals[1] and can even infect humans. Since 1914, sporadic and contentious cases of PRV infection in humans have been reported, often based on clinical symptoms, animal contact history, or antibody detection.[4,5] In China, limited by the development of diagnostic technology and clinical medical cognition, PRV infection screening was not included in most of the encephalitis cases before 2010.[6] Notably, cases of human infection with PRV resurfaced in China in 2017. Ai et al. reported the first genetically confirmed case of human PRV infection.[7] The patient exhibited symptoms including fever, headache, and progressive vision loss shortly after acute onset. Sequencing revealed a high degree of homology between the patient-derived virus strain and a prevalent highly pathogenic mutant strain in China.[8,9] Subsequent reports confirmed several cases of human PRV infection.[10−18] Liu et al. made a significant contribution by isolating a human PRV (hSD-1/2019 strain) closely related to a PRV variant for the first time.[19] These cases collectively demonstrate that the PRV variants prevalent in China have the capability to infect humans, posing a significant and underestimated threat to public health and safety.

Received: July 14, 2024
Revised: December 27, 2024
Accepted: January 13, 2025
Published: January 23, 2025

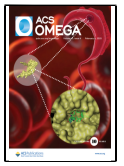

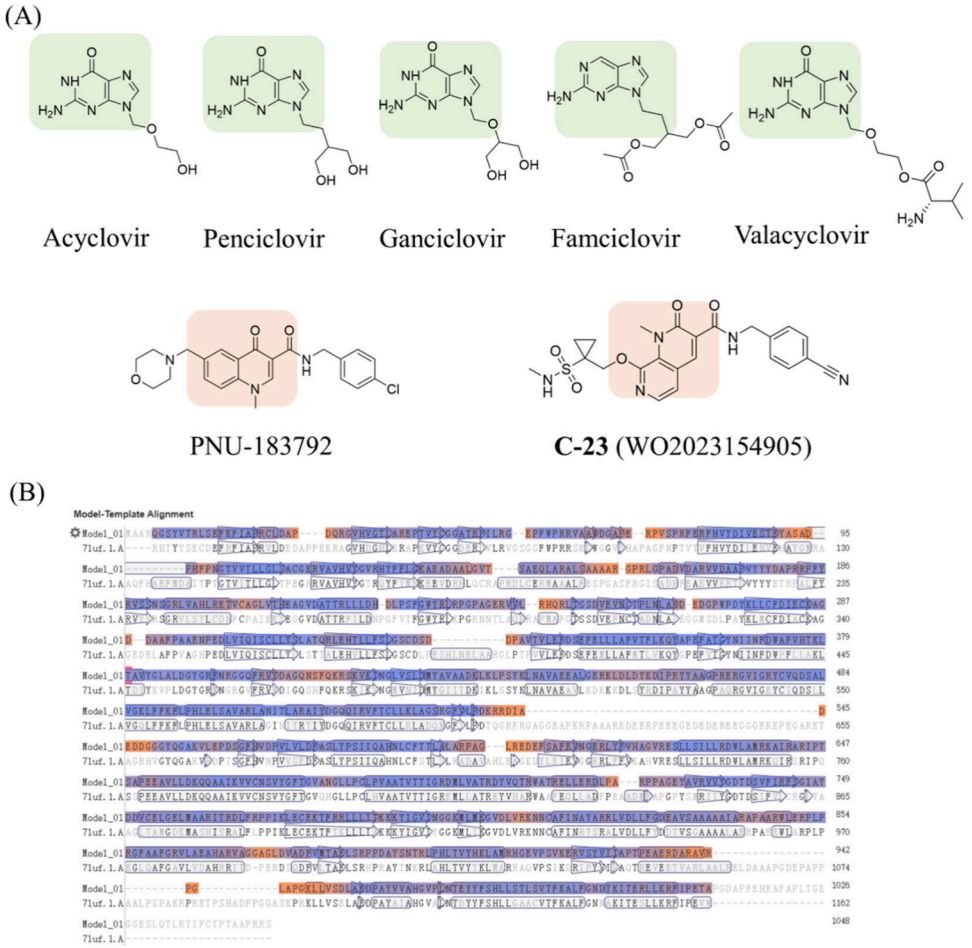

Figure 1. (A) HSV-1 inhibitors that have been approved for marketing or have been reported to target their DNA polymerase. The difference in cores was color by light green and light orange, respectively. (B) The sequences align for DNA pol between PRV and HSV-1 in SWISS-MODEL. The blue to orange gradient marks the degree of amino acid similarity, with blue indicating the same amino acid.

All cases and reports highlight the ongoing relevance and urgency of addressing the potential impact of PRV on human health. However, no medical vaccines are available for humans, and only a few studies have suggested that human infection with herpes simplex virus type 1 (HSV-1) may provide cross-protection against PRV due to structural and functional similarities between PRV gB and HSV-1 gB.[20] Therefore, we believe it is crucial to investigate anti-PRV inhibitors promptly, exploring potential pathways for human anti-PRV treatments while ensuring a reasonable margin for human safety.

As mentioned earlier, PRV and HSV-1 exhibit analogous characteristics, as they both belong to the herpesvirus family. Our investigation revealed that some of the antiviral drugs for HSV-1 (Figure 1A), such as acyclovir, penciclovir, and famciclovir, are inhibitors of DNA polymerase (DNA pol), which shares up to 60% sequence similarity with PRV DNA pol (Figure 1B). Therefore, the HSV-1 DNA pol inhibitors can be considered as potential inhibitors for PRV. In addition, to mitigate side effects like myelosuppression, nephrotoxicity, and reproductive toxicity associated with these drugs, various non-nucleoside HSV-1 DNA pol inhibitors, including PNU-183792,[21,22] **C-23** (WO2023154905),[23] have been developed (Figure 1A).

In this work, we observed a high degree of sequence similarity between HSV-1 DNA pol and PRV DNA pol. Notably, the sequence of residues around the binding pocket of PNU-183792, known to bind to HSV-1 DNA pol,[21] is identical between the two DNA polymerases. This suggests that PRV DNA pol could be a viable target for anti-PRV treatments and that HSV-1 DNA pol inhibitors may aid in the development of PRV DNA pol inhibitors. In this work, the inhibitory effect of PNU-183792 on PRV replication was confirmed. Based on the positive results of PNU-183792, we sought to expand the active compound space by discovering new potentially active compounds using a reinforcement learning artificial intelligence approach.

Reinforcement learning (RL),[24] an artificial intelligence (AI) method, has been widely used in drug design for a few years. This method can optimize decision making through interaction with environments to effectively explore the chemical space.[25,26] RL, when combined with generative models, is particularly effective in optimizing molecular structures for the biological targets, enabling the creation of novel compounds with desired properties.[27] REINVENT[27] is a powerful artificial intelligence platform for new drug design that combines generative modeling and RL, with a new version 4.0.[28] The REINVENT platform facilitates new drug discovery through strategy-based RL that optimizes molecular structures while taking exploration into account. REINVENT v2.0[29] extends this capability to include distribution-learning and goal-directed scenarios, supporting parallel calculations and transfer learning. The platform features diverse scoring components,

https://doi.org/10.1021/acsomega.4c06508
ACS Omega 2025, 10, 3389−3397

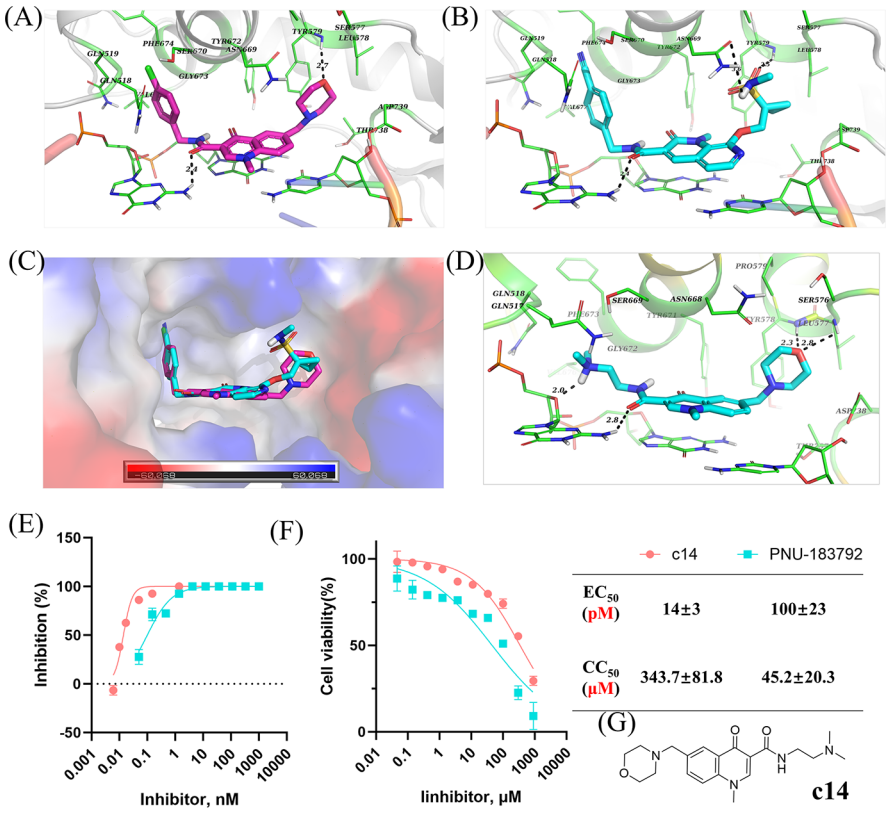

Figure 2. (A) Binding pose of PNU-183792 for PRV DNA pol. (B) Binding pose of **C-23** for PRV DNA pol. (C) Alignment for the binding pose of PNU-183792 (cyan) and **C-23** (magenta), and the surface of protein was colored according to the surface electrostatic potential. (D) Binding pose of **c14** for PRV DNA pol predicted by docking. (E) Inhibition curve for **c14** and PNU-183792 in a cell antiviral assay. (F) Cytotoxic effect curve for **c14** and PNU-183792 in a cell viability assay. (G) Structure for **c14**.

including an augmented episodic likelihood, which allows for efficient fine-tuning of generative models. In goal-directed generation, the generative model employs RL to identify and prioritize regions within the chemical space that align with the user-defined scoring functions. In our previous work,[30] a 3D scoring function was employed as a reward function, and a PI5P4K active molecular model was successfully trained using XREINVENT based on REINVENT v2.0. The previous studies have demonstrated the success of using 3D scoring functions as reward functions, leading to the identification of potentially active compounds for further validation.

In this study, we trained the DNA pol inhibitor model using the 3D function and molecular docking scoring function as reward functions. Through model sampling, we identified 21 compounds with potential activity, among which compound **c14** demonstrated significant activity at an EC_{50} of 14 pM upon validation. These compounds may represent a promising lead for the development of DNA pol inhibitors.

RESULTS AND DISCUSSION

3D Structure for PRV DNA pol. According to SWISS-MODEL analysis, the HSV-1 DNA pol (PDB ID: 7LUF) is the most suitable template due to its high homology with the PRV DNA pol. The construction of the 3D structure of PRV DNA pol was prompted based on the template provided by 7LUF. The quality assessment metrics for the model include a GMQE (Global Model Quality Estimation) of 0.77, QMEANDisCo[31] global score of 0.78 ± 0.05, and a QMEAN[32] Z-score for all atoms at −0.50 (Figure S1). This resulted in an identical structure around the nucleoside triphosphate (NTP) binding site when compared with the HSV-1 DNA pol (Figure S2), enhancing our confidence in the homologous nature of the structure. Furthermore, the result led us to hypothesize that the PRV DNA pol could serve as a potential target for anti-PRV therapy. Given the structural similarity around the NTP binding site between PRV DNA pol and HSV-1, it was postulated that inhibitors designed for the HSV-1 DNA pol NTP site might also effectively inhibit the PRV DNA pol as well. This hypothesis provides a novel framework for the development of anti-PRV therapies.

Binding Poses of PNU-183792 and C-23. The compound PNU-183792, initially sourced from 7LUF and subsequently applied to PRV DNA pol, underwent optimization through molecular dynamics (MD). The resulting binding mode, depicted in Figure 2A, reveals key interactions: its quinolone core engages in $\pi-\pi$ stacking with NTP pairs, the morpholine ring substructure forms a hydrogen bond with the backbone of TYR579, and the amide bond establishes a hydrogen bond with the anticipated pairing guanosine triphosphate (GTP). The binding mode of **C-23** (Figure 2B) was forecasted and refined via docking (Glide v9.9) and MD. This binding mode closely resembles that of PNU-183792 (Figure 2C), displaying $\pi-\pi$ stacking with NTP pairs, hydrogen bonding with the backbone of TYR579, and interaction with the GTP that will soon be paired. Furthermore, the sulfonamide segment of the structure engages in hydrogen bonding with ASN669.

PNU-183792 Can Inhibit the PRV Replication in PK15 Cells. Here, to verify our speculation, the activity of PRV replication inhibition on PK15 cells of PNU-183792 was

https://doi.org/10.1021/acsomega.4c06508
ACS Omega 2025, 10, 3389−3397

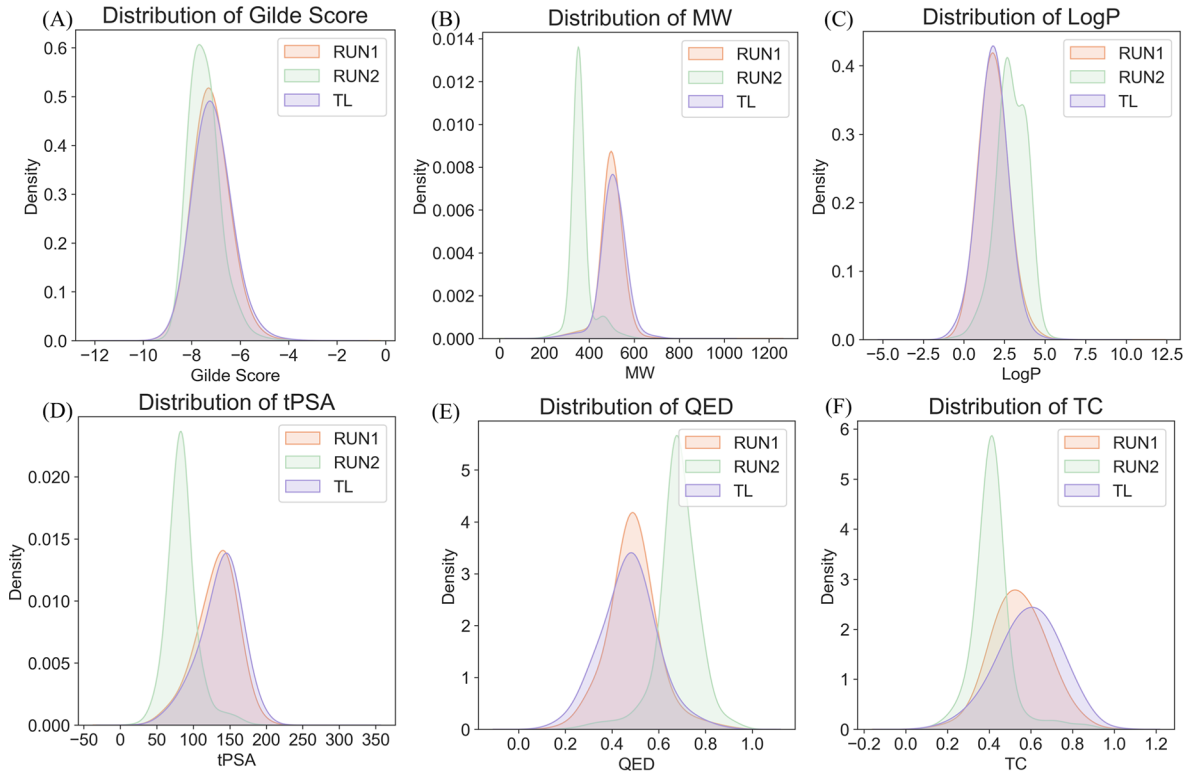

Figure 3. Density distribution plot generated by seaborn and matplotlib in python. (A) Distribution of Glide score. (B) Distribution of molecular weight. (C) Distribution of Log *P*. (D) Distribution of TPSA. (E) Distribution of QED. (F) Distribution of TC.

tested. The cellular antiviral assay results showed a concentration of 50% of maximal effect (EC_{50}) of 100 pM for PNU-183792 (Figure 2E). It exhibits significant inhibition of viral replication at a low concentration of 4.1 nM, with PRV copies of approximately 1.6×10^3 copies/μL, compared to the negative control, which showed approximately 8.1×10^6 copies/μL (Figure S3).

Transfer Learning and Reinforcement Learning. During the RL molecule generation process, two distinct tasks, namely, *RUN1* and *RUN2*, were run according to PNU-183792 and its analogs. Each task imposed unique constraints to explore the activity structure space. A total of 30,000 molecules were sampled from the final models trained by *RUN1* and *RUN2*, respectively. The efficacy of the model was evaluated throughout the learning process. As the learning process progressed, for *RUN1*, the pharmacophore constraint score tended to stabilize around 1.2, while the average score stabilized at approximately 0.25 (Figure S4A,C). Following the sampling process, 30,000 compounds were generated, with a valid SMILES rate of 98.30% and a unique molecule rate of 87.33%. Similarly, for *RUN2*, the award function for Autodock Vina score stabilized at approximately 2.0, with the average score stabilizing at approximately 0.50 (see Figure S4B,C). Following the sampling process, 30,000 compounds were generated, with a valid SMILES rate of 99.21% and a unique molecule rate of 31.11%.

Distribution for the Generated Compounds. Here, a reanalysis of molecular docking was carried out for compounds derived from both *RUN1* and *RUN2* by Glide v9.9. It was revealed that compounds from *RUN2* exhibited notably stronger binding abilities, as reflected in their Glide score distribution, spanning from −10 to −4, with a median score of close to −8. Conversely, compounds from *RUN1* also demonstrated a distribution within the same range (−10 to −4), although with a median score of around −7. It is noteworthy that both *RUN1* and *RUN2* displayed superior binding abilities compared to *TL*, which was not trained via reinforcement learning and showcased a Glide score distribution ranging from −10 to −2, with a median score approximately at −7 (Figure 3A).

Our focus on activity-related information within reinforcement learning highlights the significance of descriptors such as shape, docking score, and inherent pharmacophore model characteristics. These descriptors impose constraints on molecules during the learning process. The generated compounds are close to the rule of five (RO5) in terms of molecular weight, Log *P*, topological polar surface area (TPSA), etc. Furthermore, they exhibit a higher quantitative estimate of drug-likeness (QED) and feature more novel structures.

Nevertheless, there are notable differences between *RUN1* and *RUN2*. As for *RUN1*, the objective is to enhance potential activity with minimal alterations observed in other molecular properties. Conversely, in *RUN2*, where the learning process incorporates docking as a reward function without additional molecule restrictions, improvements in the potential activity are accompanied by changes in other molecular properties. The molecules sampled by *RUN1* and those sampled in *TL* demonstrate similar distributions of relative molecular weights, while the distributions are predominantly within the range of 200 to 800, with the main range being between 400 and 600 and a median of 500. In contrast, the molecules sampled by the *RUN2* model exhibit relative molecular weight distributions within 200−600, with a concentration primarily between 250 and 400, aligning more closely with the RO5. (Figure 3B) With regard to the distribution of Log *P*, *RUN1* is comparable

https://doi.org/10.1021/acsomega.4c06508
ACS Omega 2025, 10, 3389−3397

to *TL*, with values ranging from −2.5 to 5.0, concentrated primarily between 0 and 4, and with a median of 2. In contrast, the Log *P* distribution of *RUN2* spans from 0 to 5, with the majority between 1 and 5, with a median of 2.5. (Figure 3C). For the terms of TPSA, both *RUN1* and *TL* are distributed within the range of 50 to 200, with a median of 150. In contrast, *RUN2* spans from 20 to 200, with the majority of values falling within 50−120, with a median of 100 (Figure 3D). Assessing QED, *RUN1* displays a distribution similar to that of TL, with a broad range between 0.1 and 1.0, with a median of 0.5. Conversely, *RUN2* ranges between 0.2 and 1.0, with the majority of values falling between 0.6 and 0.8, with a median of 0.7, indicating a higher overall drug-likeness (Figure 3E). Furthermore, comparing the Tanimoto Coefficients (TCs) of the Morgan fingerprints reveals that *RUN1* exhibits higher similarity to *TL* within the training set, with a distribution between 0 and 1.0 and a median around 0.6. In contrast, *RUN2* demonstrates more novel compounds, with similarity predominantly distributed between 0.2 and 0.6 and a median at 0.4 (Figure 3F).

Details for 21 Hits after Rescreening. A manual inspection of the compounds and their binding modes was conducted, taking key parameters into account, including QED, Log *P*, TPSA, and Glide score. This analysis resulted in the identification of novel structures with potential enzymatic activity, with 11 hits originating from *RUN1* and the other 10 hits from *RUN2* (all 21 hits are shown in Table S1). Our investigation revealed that all of these compounds are capable of forming hydrogen bonds with the template base GTP in the pocket and engaging in $\pi-\pi$ stacking with paired NTP. Furthermore, some compounds exhibit the ability to form hydrogen bonds with TYR579 (**c2**, **c3**, **c4**, **c5**, **c6**, **c10**, **c11**, **c12**, **c13**, **c15**, **c17**, **c18**, **c19**, **c21**), ASP739 (**c1**, **c7**, **c19**, **c21**), and ASN669 (**c4**, **c5**, **c8**, **c17**, **c21**). Moreover, a few compounds have been identified as demonstrating potential halogen bonding interactions with GLN519 (**c1**, **c7**, **c8**, **c9**, **c11**, **c12**, **c15**, **c17**, **c20**) (Figure S5). Subsequently, MD and MM/GBSA calculations were performed for the identified hits. The lowest binding free energy (Δ*G*) was determined to be −119.65 ± 0.49 kcal/mol, indicating a significant potential advantage (Table S1).

c14 Can Significantly Inhibit the Replication of PRV. The binding pose predicted by docking of **c14** (Figure 2G) revealed a striking similarly to PNU-183792, which forms hydrogen bonds with LEU577, TYR578, and unpaired GTP and $\pi-\pi$ stacking with paired NTP. Notably, **c14** exhibited an additional interaction, interacting with the phosphoric acid in GTP with an electrostatic and hydrogen-bonding interaction (Figure 2D). The cellular antiviral assay results showed that **c14** continued to significantly inhibit viral replication at a low concentration of 1.4 nM, with PRV copies of approximately 1.4×10^3 copies/μL, compared to the black control, which showed approximately 8.1×10^6 copies/μL (Figure S3). As shown in Figure 2E, the EC_{50} for **c14** is 14 pM, demonstrating that **c14** showed superior cellular antiviral activity compared with PNU-183792 by approximately 6-fold. Furthermore, there are significantly lower viral copies observed in the **c14**-treated cell group at equivalent concentrations of PNU-183792 (Figure S3). Notably, in the reported analogs of PNU-183792 as an inhibitor of HSV-1 DNA pol, there is no electropositive group as in **c14** in the corresponding moiety (Figure S6), which may be the advantage of **c14**.

c14 Has a Wide Cellular Drug Safety Window. As shown in Figure 2F, the 50% cytotoxic concentration (CC_{50}) of **c14** is 343.7 μM, while the CC_{50} of PNU-183792 is 45.2 μM. The results of the cell viability assay of **c14** showed a high level of safety, with about an increase of 8-fold over PNU-183792. Meanwhile, compared to PNU-183792, **c14** showed higher cell viability than PNU-183792 at equivalent concentrations. Compared with the EC_{50} and CC_{50} of **c14**, it showed an approximately 20,000,000-fold drug safety margin.

CONCLUSIONS

A resurgence of PRV has been observed in certain pig farms across China, resulting in significant economic losses. Furthermore, the emergence of human infections caused by these PRV, which are characterized by more severe symptoms, represents a growing concern. Consequently, the necessity for research into prevention and treatment strategies against PRV strains cannot be overstated.

In this study, we capitalized on the striking similarity between PRV DNA pol and the HSV-1 DNA pol. This led us to experimentally verify the inhibitory potential of PNU-183792, a non-nucleoside inhibitor of HSV-1, against PRV replication in cell assays, revealing an impressive EC_{50} of 100 pM. This groundbreaking result serves as a cornerstone for our ongoing investigations into PRV inhibitors. Moreover, it is worth noting that other HSV-1 DNA pol inhibitors may also exhibit similar effectiveness. There have been domestic attempts to use acyclovir against human PRV infection.[10,15−18] Of course, more exploration is needed for use in emergency situations where no specific drug is currently available.

Furthermore, by leveraging a multidisciplinary approach combining reinforcement learning, 3D pharmacophore modeling, and Autodock Vina docking as reward functions, we identified several promising lead compounds. Notably, compound **c14** emerged as a standout candidate, exhibiting exceptional activity and safety profiles with an EC_{50} of 14 pM and a CC_{50} of 343.7 uM. This remarkable finding positions **c14** as a highly promising lead compound, laying a solid foundation for future drug discovery and development endeavors targeting PRV.

COMPUTATIONAL AND EXPERIMENTAL SECTION

Homology Modeling and Molecular Dynamics (MD) Simulation for RPV DNA pol. The 3D structure of PRV DNA pol for the HuBXY/2018 strain (Sequence ID: QMP81333.1) was generated through homology modeling by SWISS-MODEL[33−37] (https://swissmodel.expasy.org/), with the template being HSV-1 DNA pol (PDB ID: 7LUF), showing a sequence similarity of 60%. Subsequently, the PRV DNA pol structure obtained was aligned with 7LUF, and the DNA and PNU-183792 molecules were merged from 7LUF into the PRV DNA pol structure. The 100 ns molecular dynamics relaxation was performed for the complexes of PNU-183792 and RPV DNA pol, following the settings in our previous work.[30] After MD, one frame was selected every 5 frames within the last 5 ns, and the average structure derived from these selections was regarded as the relaxed 3D structure of PRV DNA pol.

Molecular Docking and MD for C-23. C-23 was docked into PRV DNA pol by Induced Fit Docking (@Schrödinger v2023−2), with the pockets generated based on the ligand PNU-183792. The docking precision was set to SP, while other

https://doi.org/10.1021/acsomega.4c06508
ACS Omega 2025, 10, 3389−3397

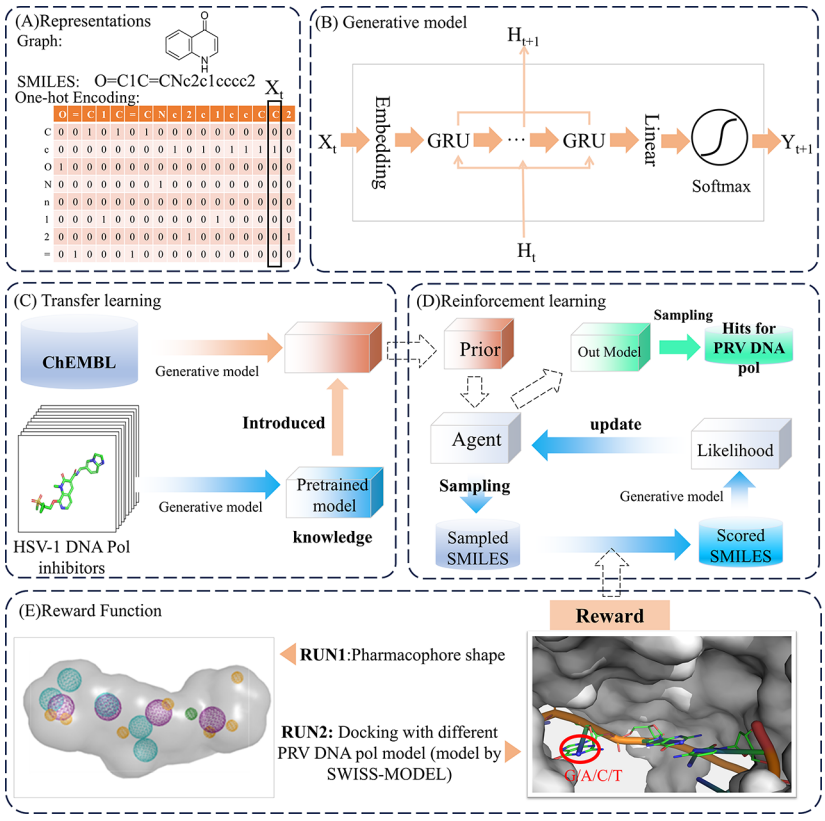

Figure 4. Transfer learning and reinforcement learning for PRV DNA pol hit discovery. (A) The molecules were represented by SMILES and one-hot encoding. (B) The generative model. (C) Transfer learning. (D) Reinforcement learning. (E) Reward functions.

parameters were maintained at default settings. The top-ranked pose, determined through scoring and manual inspection, was deemed a plausible conformation.

Transfer Learning and Reinforcement Learning. TL and RL are both integral components of the framework of XREINVENT. Here, the molecules were represented by SMILES and one-hot encoding (Figure 4A), and the generative model was built by Gated Recurrent Unit (GRU)[38] (Figure 4B). Transfer learning was employed to generate prior models (Figure 4C), with source models consistent with previous studies,[30] all of which were trained on the ChEMBL compound library. Subsequently, the compounds from the patent for PNU-183792[22] and **C-23**[23] serve as the target compound data set for refinement. This process created a focused prior, enhancing the likelihood of the model generating compounds resembling those in the target data set. Following this, two distinct 500-step reinforcement learning sessions were then conducted for goal-directed scenarios (Figure 4D) (for more details, see Supporting Information Part 2). Here, scoring based on pharmacophore (set according the poses of **C-23**, more details see Supporting Information Part 3) and molecular docking (by Autodock Vina) was set as reward functions, respectively (Figure 4E). The "focused prior" was employed as a generative model, accelerating the RL process by enhancing the likelihood of producing relevant compounds compared to using a general, unfocused prior as an agent.

Rescreening for the Compounds Generated by XREINVENT. The SMILES for the compounds generated by XREINVENT were converted to a three-dimensional (3D) conformation by LigPrep v3 in Schrödinger v2023−2 and the protonation states, and isomers were determined by Epik.v6.4. Then the conformers with the lowest energy for each molecule were retained for docking. Then the compounds were rescreened by two steps. (1) Docking by Glide v9.9 in Schrödinger v2023−2 with HTVS precision. The pocket was determined according to the binding pose of PNU-183792. During the docking protocol employed in RL, for the same small molecule, the nucleoside triphosphates (NTPs) that are about to be paired inside the pocket are set to A, C, T, and U, respectively, and 4 dockings will be performed. The scoring corresponding to the lowest scoring value (indicating the strongest binding affinity) was considered to be the binding affinity of the molecule. Five conformations were generated per molecule per docking. (2) Visual inspection. The compounds for the top 1000 poses which can form two or more hydrogen bonds and π interactions or other types of interactions with additional active site residues, such as TYR579, ASN669, and NTP, remained. (3) The poses for the remaining compounds were relaxed by MD and the binding energy predicted by Molecular Mechanics/Generalized Born Surface Area (MM/GBSA). It was carried out in AMBER20, and the steps were the same as our previous work.[30]

Chemistry. Unfortunately, we were unable to synthesize these molecules in the 21 potential hits, except for **c14**. The synthetic routes for compounds **c14** (*N*-(2-(dimethylamino)-ethyl)-1-methyl-6-(morpholinomethyl)-4-oxo-1,4-dihydroquinoline-3-carboxamide) and PNU-183792 (*N*-(4-chlorobenzyl)-1-methyl-6-(morpholinomethyl)-4-*oxo*-1,4-dihydroquinoline-3-carboxamide) are illustrated in Supporting Information Part 4. The structures of the synthesized compounds were characterized by ^{1}H NMR, ^{13}C NMR (just for **c14**) spectroscopy, and HRMS. All the final products were obtained

https://doi.org/10.1021/acsomega.4c06508
ACS Omega 2025, 10, 3389−3397

in high purity (95%) by high performance liquid chromatography.

Cells and Virus. PK15 cells were stored in our laboratory[39] and cultured with fresh Dulbecco's modified Eagle's medium (DMEM) (No. 11965092, Gibco) with 10% fetal bovine serum (FBS) (No. P30−3306, PAN) and 1% penicillin-streptomycin solution (100X, No. BL505A, Biosharp) at 37 °C, incubated at a mixture of 5% CO_2 and 95% atmosphere. PRV was isolated from a pig farm in Hubei Province, China, whose DNA pol was identical with that of the HuBXY/2018 strain.

Cell Antiviral Assay. PK15 cells, at 80% confluence, were seeded in 96-well plates. After 24 h the culture medium was discarded, and the cells were washed three times with PBS. Fresh DMEM containing 2% FBS and 1% penicillin-streptomycin solution (100 μL) was added, and the cells were incubated at 37 °C for 4 h. Then the cells were treated with various concentrations of **c14** or PNU-183792 (1000 nM, 333.3 nM, 111.1 nM, 37.0 nM, 12.4 nM, 4.1 nM, 1.4 nM, 0.46 nM, 0.15 nM, 0.05 nM, 0.017 nM, 0.010 nM, and 0.006 nM) for 2 h. The inhibitors were prepared by dissolving **c14** or PNU-183792 in DMSO to a concentration of 10 mM and then diluted in DMEM to the desired concentrations (100 times of the target concentration), with 1 μL of the solution added to each well. The control group was treated with 1 μL of 1% DMSO in DMEM. After treatment, the cells were then infected with PRV (MOI = 1). 48 h later, and total DNA was extracted using phenol-chloroform (Solarbio Bioscience & Technology Co., Ltd.). Target genes were amplified by SYBR green-based quantitative PCR (qPCR) using 2 × Taq Master Mix (Vazyme, Nanjing, China). The primers used in this study are listed in Table 1. The inhibition rate of the experimental group was calculated by

Table 1. Primer Sequences for qPCR

Name	Sequence
gB-1	GCGGCATCGCCAACTTCTTCC
gB-2	GCCTCGTCCACGTCGTCCTCTT

$$\text{Inhibition rate} = \left(1 - \frac{\text{number of virus copies in experimental group}}{\text{number of virus copies in positive group}}\right) \times 100\%$$

The EC_{50} was fitted by GraphPad Prism 9.

Cell Viability Assay. Cell viability was determined using the CCK-8 reagent assay (No. BL1055B, Biosharp). Briefly, PK15 cells proceeded at 80% confluence in 96-well plates, and 12 h later, the cells were treated with various concentrations of **c14** or PNU-183792 (900 μM, 300 μM, 100 μM, 33.3 μM, 11.1 μM, 3.7 μM, 1.23 μM, 0.41 μM, 0.14 μM, and 0.05 μM). The inhibitors were prepared the same as in the cell antiviral assay. The control group was treated with 1 μL of 1% DMSO in DMEM. 72 h later, CCK-8 reagent was added with 10 μL per well and incubated at 37 °C for 2 h. The optical density was measured at a wavelength of 450 nm by an Envision 2105, PerkinElmer. The results were plotted as % of cell viability in the treated group compared to the control group. The CC_{50} was fitted by GraphPad Prism 9.

■ ASSOCIATED CONTENT

Data Availability Statement

All data generated or analyzed during the current study are included in this article and Supporting Information. The XREINVENT was obtained from Github (https://github.com/weilin199204/xdalgorithm_XtalPi_copy). The input files, training data sets, and out models for *TL*, *RUN1*, and *RUN2* are available at Zenodo (https://zenodo.org/records/12560194).

Supporting Information

The Supporting Information is available free of charge at https://pubs.acs.org/doi/10.1021/acsomega.4c06508.

Details of the results, methods of chemical synthesis, and ^{1}H NMR spectroscopy and HRMS (PDF)

Detailed data for 3000 compounds generated by *RUN1* and *RUN2* (ZIP)

■ AUTHOR INFORMATION

Corresponding Author

Zigong Wei − *State Key Laboratory of Biocatalysis and Enzyme Engineering, School of Life Sciences, Hubei University, Wuhan, Hubei 430061, PR China; Hubei Jiangxia Laboratory, Wuhan, Hubei, PR China; Hubei Province Key Laboratory of Biotechnology of Chinese Traditional Medicine, National & Local Joint Engineering Research Center of High-throughput Drug Screening Technology, School of life sciences, Hubei University, Wuhan, Hubei 430061, PR China;* orcid.org/0000-0002-2445-6171; Email: weizigong@163.com, weizigong@hubu.edu.cn

Authors

Lin Wei − *State Key Laboratory of Biocatalysis and Enzyme Engineering, School of Life Sciences, Hubei University, Wuhan, Hubei 430061, PR China;* orcid.org/0000-0002-1977-2700

Yang Hu − *State Key Laboratory of Biocatalysis and Enzyme Engineering, School of Life Sciences, Hubei University, Wuhan, Hubei 430061, PR China*

Licheng Bai − *State Key Laboratory of Biocatalysis and Enzyme Engineering, School of Life Sciences, Hubei University, Wuhan, Hubei 430061, PR China*

Chenxu Xiao − *State Key Laboratory of Biocatalysis and Enzyme Engineering, School of Life Sciences, Hubei University, Wuhan, Hubei 430061, PR China*

Zhang Liu − *State Key Laboratory of Biocatalysis and Enzyme Engineering, School of Life Sciences, Hubei University, Wuhan, Hubei 430061, PR China*

Yun You − *State Key Laboratory of Biocatalysis and Enzyme Engineering, School of Life Sciences, Hubei University, Wuhan, Hubei 430061, PR China*

Keke Wang − *State Key Laboratory of Biocatalysis and Enzyme Engineering, School of Life Sciences, Hubei University, Wuhan, Hubei 430061, PR China*

Yunyuan Huang − *Hubei Key Laboratory of Genetic Regulation and Integrative Biology, School of Life Sciences, Central China Normal University, Wuhan, Hubei 430079, PR China*

Junfei Zhu − *State Key Laboratory of Biocatalysis and Enzyme Engineering, School of Life Sciences, Hubei University, Wuhan, Hubei 430061, PR China*

https://doi.org/10.1021/acsomega.4c06508
ACS Omega 2025, 10, 3389−3397

Jun Weng − *State Key Laboratory of Biocatalysis and Enzyme Engineering, School of Life Sciences, Hubei University, Wuhan, Hubei 430061, PR China; Key Laboratory of Molecular Biophysics of Ministry of Education, College of Life Science and Technology, Huazhong University of Science and Technology, Wuhan, Hubei 430074, PR China*

Wenling Zhou − *State Key Laboratory of Biocatalysis and Enzyme Engineering, School of Life Sciences, Hubei University, Wuhan, Hubei 430061, PR China*

Han Li − *State Key Laboratory of Biocatalysis and Enzyme Engineering, School of Life Sciences, Hubei University, Wuhan, Hubei 430061, PR China*

Honghe Zhao − *State Key Laboratory of Biocatalysis and Enzyme Engineering, School of Life Sciences, Hubei University, Wuhan, Hubei 430061, PR China*

Zhiyong Wu − *State Key Laboratory of Biocatalysis and Enzyme Engineering, School of Life Sciences, Hubei University, Wuhan, Hubei 430061, PR China*

Meng Mei − *State Key Laboratory of Biocatalysis and Enzyme Engineering, School of Life Sciences, Hubei University, Wuhan, Hubei 430061, PR China*

Complete contact information is available at: https://pubs.acs.org/10.1021/acsomega.4c06508

Author Contributions

[#]Lin Wei, Yang Hu and Licheng Bai contributed equally to this study. Lin Wei, Yang Hu, Licheng Bai, Chenxu Xiao, Junfei Zhu and Jun Weng performed the methodology; Lin Wei, Yang Hu, Licheng Bai, Chenxu Xiao, Zhang Liu, Yun You, Keke Wang, Wenling Zhou, Han Li and Honghe Zhao performed the validation; Zigong Wei and Yunyuan Huang were responsible for the resources; Lin Wei and Yunyuan Huang ran the software; Lin Wei and Yang Hu performed visualization; Lin Wei, Junfei Zhu, Jun Weng, Meng Mei and Zigong Wei supervised; Lin Wei, Yunyuan Huang, Jun Weng and Zigong Wei performed funding acquisition. In addition, Lin Wei was responsible for conceptualization, data curation and project administration; Lin Wei wrote the original draft of the manuscript; and all coauthors provided editorial comments and review.

Funding

This work was supported by the National Key R&D Program of China (2023YFE0110100), Hubei Provincial Natural Science Foundation of China (2024AFB465), State Key Laboratory Open Project (SKLBEE2022007) from State Key Laboratory of Biocatalysis and Enzyme Engineering and Enzyme Engineering, and self-determined research funds of Central China Normal University from the colleges' basic research and operation of Ministry of Education (CCNU24ai006).

Notes

The authors declare no competing financial interest.

■ ACKNOWLEDGMENTS

We thank the HPC center at State Key Laboratory of Biocatalysis and Enzyme Engineering for cloud computing support. We also thank Dr. Shuangli Li, Innovation Academy for Precision Measurement Science and Technology, CAS, for 600 M NMR instruments.

■ ABBREVIATIONS

PRV, pseudorabies virus; HSV-1, herpes simplex virus type 1; DNA pol, DNA polymerase; RL, reinforcement learning; AI, artificial intelligence; NTP, nucleoside triphosphate; MD, molecular dynamics; GMQE, Global Model Quality Estimation; GTP, guanosine triphosphate; RO5, rule of five; TPSA, topological polar surface area; QED, quantitative estimate of drug-likeness; TL, transfer learning; CCK-8, Cell Counting Kit-8

■ REFERENCES

(1) Pomeranz, L. E.; Reynolds, A. E.; Hengartner, C. J. Molecular biology of pseudorabies virus: impact on neurovirology and veterinary medicine. *Microbio. Mol. Biol. Rev.* **2005**, *69*, 462−500.

(2) Sun, Y.; Luo, Y.; Wang, C. H.; Yuan, J.; Li, N.; Song, K.; Qiu, H. J. Control of swine pseudorabies in China: Opportunities and limitations. *Vet. Microbiol.* **2016**, *183*, 119−124.

(3) Gao, X.; Zheng, H.; Zou, M.; Liu, S.; Liu, L.; Fan, G.; Wu, F. Serological Investigation of Porcine Pseudo-Rabies on Intensive Swine Farms From 2012 To 2017 In China. *Chin. J. Ani. Infect. Dis.* **2018**, *28*, 87−90.

(4) Schükrü-Aksel, I.; Tunçman, Z. Aujeskysche Erkrankung in der Türkei bei Mensch und Tier. *Zeitschrift für die gesamte Neurologie und Psychiatrie* **1940**, *169*, 598−606.

(5) Hanson, R. P. The history of pseudorabies in the United States. *J. Am. Vet. Med. Assoc.* **1954**, *124*, 259−261.

(6) Guo, Z.; Chen, X.; Zhang, G. Human PRV Infection in China: An Alarm to Accelerate Eradication of PRV in Domestic Pigs. *Virol. Sin.* **2021**, *36*, 823−828.

(7) Ai, J.; Weng, S.; Cheng, Q.; Cui, P.; Li, Y.; Wu, H.; Zhu, Y.; Xu, B.; Zhang, W. Human Endophthalmitis Caused By Pseudorabies Virus Infection, China, 2017. *Emerg. Infect. Dis.* **2018**, *24*, 1087−1090.

(8) Ye, C.; Guo, J. C.; Gao, J. C.; Wang, T. Y.; Zhao, K.; Chang, X. B.; Wang, Q.; Peng, J. M.; Tian, Z. J.; Cai, X. H.; et al. Genomic analyses reveal that partial sequence of an earlier pseudorabies virus in China is originated from a Bartha-vaccine-like strain. *Virology* **2016**, *491*, 56−63.

(9) Luo, Y.; Li, N.; Cong, X.; Wang, C.; Du, M.; Li, L.; Zhao, B.; Yuan, J.; Liu, D.; Li, S.; et al. Pathogenicity and genomic characterization of a pseudorabies virus variant isolated from Bartha-K61-vaccinated swine population in China. *Vet. Microbiol.* **2014**, *174*, 107−115.

(10) Zhao, W.; Wu, Y.; Li, H.; Li, S.; Fan, S.; Wu, H.; Li, Y.; Lv, Y.; Han, J.; Zhang, W.; et al. Clinical experience and next-generation sequencing analysis of encephalitis caused by pseudorabies virus. *Natl. Med. J. China* **2018**, *98*, 1152−1157.

(11) Hou, Y.; Wang, Y.; Zhang, Y.; Yu, H.; Zhao, Y.; Yi, A. Human Encephalitis Caused by Pseudorabies Virus in China: A Case Report and Systematic Review. *Vector-Borne Zoonot.* **2022**, *22*, 391−396.

(12) Wang, D.; Tao, X.; Fei, M.; Chen, J.; Guo, W.; Li, P.; Wang, J. Human encephalitis caused by pseudorabies virus infection: a case report. *J. Neurovirol.* **2020**, *26*, 442−448.

(13) Wang, Y.; Nian, H.; Li, Z.; Wang, W.; Wang, X.; Cui, Y. Human encephalitis complicated with bilateral acute retinal necrosis associated with pseudorabies virus infection: A case report. *Int. J. Infect. Dis.* **2019**, *89*, 51−54.

(14) Xu, G.; Hou, B.; Xue, C.; Xu, Q.; Qu, L.; Hao, X.; Liu, Y.; Wang, D.; Li, Z.; Jin, X. Acute Retinal Necrosis Associated with Pseudorabies Virus Infection: A Case Report and Literature Review. *Ocul. Immunol. Inflamm.* **2023**, 1−8.

(15) Yan, W.; Hu, Z.; Zhang, Y.; Wu, X.; Zhang, H. Case Report: Metagenomic Next-Generation Sequencing for Diagnosis of Human Encephalitis and Endophthalmitis Caused by Pseudorabies Virus. *Front. Med.* **2022**, DOI: 10.3389/fmed.2021.753988.

(16) Yang, H.; Han, H.; Wang, H.; Cui, Y.; Liu, H.; Ding, S. A Case of Human Viral Encephalitis Caused by Pseudorabies Virus Infection in China. *Front. Neurol.* **2019**, *10*, 534.

(17) Yue, L.; Yi, L.; Fei, T.; MengWu, T.; Man, L.; LiQing, W.; YueLi, Z.; JiaLiang, D.; Hui, B.; JunYing, H. Human Encephalitis Complicated With Ocular Symptoms Associated With Pseudorabies Virus Infection: A Case Report. *Front. Neurol.* **2022**, *13*, 878007.
(18) Zheng, L.; Liu, X.; Yuan, D.; Li, R.; Lu, J.; Li, X.; Tian, K.; Dai, E. Dynamic cerebrospinal fluid analyses of severe pseudorabies encephalitis. *Transbound. Emerg. Dis.* **2019**, *66*, 2562−2565.
(19) Liu, Q.; Wang, X.; Xie, C.; Ding, S.; Yang, H.; Guo, S.; Li, J.; Qin, L.; Ban, F.; Wang, D.; et al. A Novel Human Acute Encephalitis Caused by Pseudorabies Virus Variant Strain. *Clin. Infect. Dis.* **2021**, *73*, No. e3690.
(20) Robbins, A. K.; Dorney, D. J.; Wathen, M. W.; Whealy, M. E.; Gold, C.; Watson, R. J.; Holland, L. E.; Weed, S. D.; Levine, M.; Glorioso, J. C. The pseudorabies virus gII gene is closely related to the gB glycoprotein gene of herpes simplex virus. *J. Virol.* **1987**, *61*, 2691−2701.
(21) Hayes, R. P.; Heo, M. R.; Mason, M.; Reid, J.; Burlein, C.; Armacost, K. A.; Tellers, D. M.; Raheem, I.; Shaw, A. W.; Murray, E.; et al. Structural understanding of non-nucleoside inhibition in an elongating herpesvirus polymerase. *Nat. Commun.* **2021**, *12*, 3040.
(22) Turner, S. R.; Strohbach, J. W.; Thaisrivongs, S.; Vaillancourt, V. A.; Schnute, M. E.; Scott, A. 4-oxo-1,4-dihydro-3-quinolinecarboxamides As Antiviral Agents. WO0040563, 2000.
(23) Aktoudianakis, E.; Corkey, B. K.; Franke, J. M.; Germek, I. F.; Hudlicky, J. R.; Kalla, R. V.; Lu, P.; Mcauley, E. P.; Metobo, S. E.; Moreau, R. J., et al. Antiviral Pyrazolopyridinone Compounds. WO2023154905, 2023.
(24) Sutton, R. S.; Barto, A. G. Reinforcement Learning: An Introduction. *IEEE Trans. Neural Networks* **1998**, *9*, 1054.
(25) Blaschke, T.; Engkvist, O.; Bajorath, J.; Chen, H. Memory-assisted reinforcement learning for diverse molecular de novo design. *J. Cheminf.* **2020**, *12*, 68.
(26) Liu, X.; Ye, K.; van Vlijmen, H. W. T.; Ijzerman, A. P.; van Westen, G. J. P. An exploration strategy improves the diversity of de novo ligands using deep reinforcement learning: a case for the adenosine A2A receptor. *J. Cheminf.* **2019**, *11*, 35.
(27) Olivecrona, M.; Blaschke, T.; Engkvist, O.; Chen, H. Molecular de-novo design through deep reinforcement learning. *J. Cheminf.* **2017**, *9*, 48.
(28) Loeffler, H. H.; He, J.; Tibo, A.; Janet, J. P.; Voronov, A.; Mervin, L. H.; Engkvist, O. Reinvent 4: Modern AI-driven generative molecule design. *J. Cheminf.* **2024**, *16*, 20.
(29) Blaschke, T.; Arus-Pous, J.; Chen, H.; Margreitter, C.; Tyrchan, C.; Engkvist, O.; Papadopoulos, K.; Patronov, A. REINVENT 2.0: An AI Tool for De Novo Drug Design. *J. Chem. Inf. Model.* **2020**, *60*, 5918−5922.
(30) Wei, L.; Xu, M.; Liu, Z.; Jiang, C.; Lin, X.; Hu, Y.; Wen, X.; Zou, R.; Peng, C.; Lin, H.; et al. Hit Identification Driven by Combining Artificial Intelligence and Computational Chemistry Methods: A PI5P4K-β Case Study. *J. Chem. Inf. Model.* **2023**, *63*, 5341−5355.
(31) Studer, G.; Rempfer, C.; Waterhouse, A. M.; Gumienny, R.; Haas, J.; Schwede, T. QMEANDisCo-distance constraints applied on model quality estimation. *Bioinformatics* **2020**, *36* (6), 1765−1771.
(32) Benkert, P.; Biasini, M.; Schwede, T. Toward the estimation of the absolute quality of individual protein structure models. *Bioinformatics* **2011**, *27* (3), 343−350.
(33) Waterhouse, A.; Bertoni, M.; Bienert, S.; Studer, G.; Tauriello, G.; Gumienny, R.; Heer, F. T.; de Beer, T. A. P.; Rempfer, C.; Bordoli, L.; et al. SWISS-MODEL: homology modelling of protein structures and complexes. *Nucleic Acids Res.* **2018**, *46*, W296−W303.
(34) Bertoni, M.; Kiefer, F.; Biasini, M.; Bordoli, L.; Schwede, T. Modeling protein quaternary structure of homo- and hetero-oligomers beyond binary interactions by homology. *Sci. Rep.* **2017**, *7*, 10480.
(35) Bienert, S.; Waterhouse, A.; de Beer, T. A.; Tauriello, G.; Studer, G.; Bordoli, L.; Schwede, T. The SWISS-MODEL Repository-new features and functionality. *Nucleic. Acids. Res.* **2017**, *45*, D313−D319.
(36) Guex, N.; Peitsch, M. C.; Schwede, T. Automated comparative protein structure modeling with SWISS-MODEL and Swiss-PdbViewer: a historical perspective. *Electrophoresis* **2009**, *30*, S162−S173.
(37) Studer, G.; Rempfer, C.; Waterhouse, A. M.; Gumienny, R.; Haas, J.; Schwede, T. QMEANDisCo-distance constraints applied on model quality estimation. *Bioinformatics* **2020**, *36*, 1765−1771.
(38) Chung, J.; Gulcehre, C.; Cho, K.; Yoshua, B. Empirical Evaluation of Gated Recurrent Neural Networks on Sequence Modeling. *arXiv:1412.3555v1* **2014**, DOI: 10.48550/arXiv.1412.3555.
(39) Tang, B.; Liang, H.; Zhao, P.; Wei, Z. miR-194b-3p partially inhibits Streptococcus equi subsp. zooepidemicus adherence to PK15 cells. *Vet. Microbiol.* **2017**, *210*, 38−42.

https://doi.org/10.1021/acsomega.4c06508
ACS Omega 2025, 10, 3389−3397